Localization of Impact Damage in Thin-Walled Composite Structure Using Variance-Based Continuous Wavelet Transform

R. Janeliukstis, S. Rucevskis, M.A. Sumbatyan and A. Chate

Abstract This work is focused on damage localization in thin-walled two-dimensional composite structures. A two-stage low-velocity impact damage with severities of 5 and 9 J is applied to CFRP plate in different positions and a dynamic vibration test is conducted in order to extract the resonance frequencies and corresponding deflection shapes of the structure before and after each stage of damage. Deflection shapes serve as an input for spatial continuous wavelet transform in two dimensions to calculate the damage index and standardize it for every wavelet function. Overall, 16 wavelet functions are used with scale parameters ranging from 1 till 16. The nontrivial problem of scale selection is avoided by computing the variance of normalized scalogram (VNS) over all the scales of consideration for every wavelet. Cross-correlation of VNS values between all the wavelets is performed to reveal the wavelet pairs of similar performance. These wavelet pairs are selected to compute the average VNS (AVNS). Later, a universal threshold is applied to filter the peaks of AVNS to yield the location of damage for each case of severity. Results suggest that a damage can be localized without the consideration of a specific wavelet and scale parameter.

Keywords Damage · Wavelet · Variance · Scale · Correlation · Impact · Composite · Deflection shape · Universal threshold · Plate · Scalogram

1 Introduction

Although composite materials are promising substitutes for metals, ceramics and polymers in many applications due to such qualities as high specific strength, stiffness, corrosion resistance and tailorable properties, they are vulnerable to

R. Janeliukstis (✉) · S. Rucevskis · A. Chate
Riga Technical University, Riga, Latvia
e-mail: Rims.Janeliukstis_1@rtu.lv

M.A. Sumbatyan
I.I. Vorovich Institute of Mathematics Mechanics and Computer Sciences,
Southern Federal University, Rostov-on-Don, Russia

E.N. Barkanov et al. (eds.), *Non-destructive Testing and Repair of Pipelines*,
Engineering Materials, DOI 10.1007/978-3-319-56579-8_6

various failure modes, such as matrix cracking, debonding, and delamination. The studies of low-velocity impact are important in case of composite materials because impact is one of the main failure modes of composites in through-thickness direction [1].

Numerous studies have been conducted on the effect of impact on composite materials [2–5]. Stelldinger et al. [2] found that existence of rubber layers between plies in carbon/epoxy laminate decreases the impact damage, while Topac et al. [3] used high-speed camera to record the evolution of impact fracture in CFRP laminate beam. Toivola et al. [4] observed that a combination of epoxy with a curing agent tetreglycidyl-4′-4 diaminodiphenylmethane with diethylenetriamine produces fluorescence phenomena when an epoxy resin system is subjected to impact, thus revealing even barely visible damage. Li et al. [5] detected presence of impact in CFRP structure using infrared thermography.

It is of crucial importance not only to detect presence of damage, but also to determine its location. Touching these issues is a vital part of Structural Health Monitoring (SHM) area that has only relatively recently established as a stand-alone branch of engineering. Among many damage identification methods of SHM, those that are the most widely used, are based on dynamic response of the structure. The underlying idea behind these methods is that the stiffness of the structure decreases locally in the region of damage. The dynamic parameters, mostly resonance frequencies and deflection shapes of the structure are extracted and subjected to some transformation in order to either detect damage or, taking a one step further, localize it. These methods for example are: Modal Curvature (MC) [6–10], Modal Flexibility (MF) [6, 11] and Modal Strain Energy (MSE) [11, 12] methods. In MC-based approach, one calculates the second derivative of mode shape and calculates its distribution over length of a beam or surface of a plate. Highest peaks indicate the location of damage. MF and MSE methods are based on the fact that presence of damage alters the structural parameters of flexibility (decreases) and strain energy, when structure deforms in its deflection shapes, respectively. The drawback of MC, MF, and MSE methods is that there is a necessity in reference data of undamaged structure to which the data obtained from a damaged structure is compared and their difference or ratio is expressed as a damage index.

Apart from the damage localization methods stated above, lately the most attention is directed to the Wavelet Transform (WT) method and its different modifications, which mainly include Continuous WT, Discrete WT, and also Wavelet Packet Transform (WPT) methods. This attention is justified by the fact that the WT methods do not require a reference information on a healthy structure and one can localize damage using data exclusively from a damaged structure. Large number of studies are devoted to damage localization in beam and plate structures using WT. Particular interest lies in damage localization in composite plates as those are widely used in advanced structures and vehicles. Vast studies on this subject have been conducted by Katunin et al. [13–17]. In [13], a crack damage was identified in a CFRP laminate rotor blade with complex nonlinear geometry. The conclusion was that the Discrete WT using B-spline wavelet function provided the best damage identification results. In [14] and [15], laminated polymer

composite plates with an artificial damage were considered and their mode shapes were used in damage localization using two-dimensional WT applying fractional B-spline wavelets with continuous parametric optimization. Study [16] was devoted to low-velocity impact damage localization in composite plates. Mode shapes were measured and used as an input data in the Discrete WT. Results suggested that quincunx nonseparable wavelets were able to detect even damage of low energy (different diameter impactors were used). These results were also supported with ultrasonic C-scans. In [17] honeycomb sandwich composite plates were subjected to typical composite damage, such as delaminations, cracks of a core and sheets and impact damages. Two-dimensional Discrete WT was performed on mode shapes of the plates and damage was successfully localized. Damage localization in composite plates was also conducted in [18], where two-dimensional Continuous WT was compared with two-dimensional Strain Energy and two-dimensional Gapped Smoothing methods and proved to be superior in terms of immunity to noise and reduced sensor data. Huang et al. [19] performed two-dimensional Continuous WT of a strain data of a loaded simply supported plate with integrated sensor network. Conclusion was that the method was not only able to locate damage but also to assess its severity. Yan et al. [20] investigated the possibility to detect damage in epoxy/glass fiber composite laminate plate with embedded piezoelectric actuator and sensors. Structural response was decomposed using WPT and damage was successfully detected.

In present study, a CFRP plate with two successive impact damages (5 and 9 J) is considered. Dynamic vibration test is applied to estimate resonance frequencies and deflection shapes of the plate at free boundary conditions before and after each stage of damage. The measured mode shapes are used in damage localization algorithm involving the two-dimensional Continuous Wavelet Transform. Normalized wavelet scalogram is computed and its variance is calculated with respect to scale parameter, thus excluding scales from further computations. Reference data of healthy structure are not required, but also no need to select a particular wavelet for the analysis. It is due to a cross-correlation between variances of normalized wavelet scalograms of all the wavelets is performed in order to track down the wavelet pairs of similar performance. These pairs are selected and used in calculation of a damage index distribution over the surface of the plate. Then, the universal threshold is applied to extract insignificant values do not connected with damage. The final results suggest that the proposed damage identification procedure allows for approximate damage localization of relatively small severities.

2 Experimental Vibration Testing

A specimen considered in this study is a CFRC plate laminate with the lay-up [90/0/0/45/−45/−45/45/0/90/90/0/45/−45/−45/45/0/90] containing 17 plies with the following physical parameters (Table 1):

Table 1 Physical properties of CFRP laminate plate

Length (m)	Width (m)	Thickness (m)	Mass (kg)	Density (kg/m^3)
0.359	0.1	0.0021	0.11595	1538

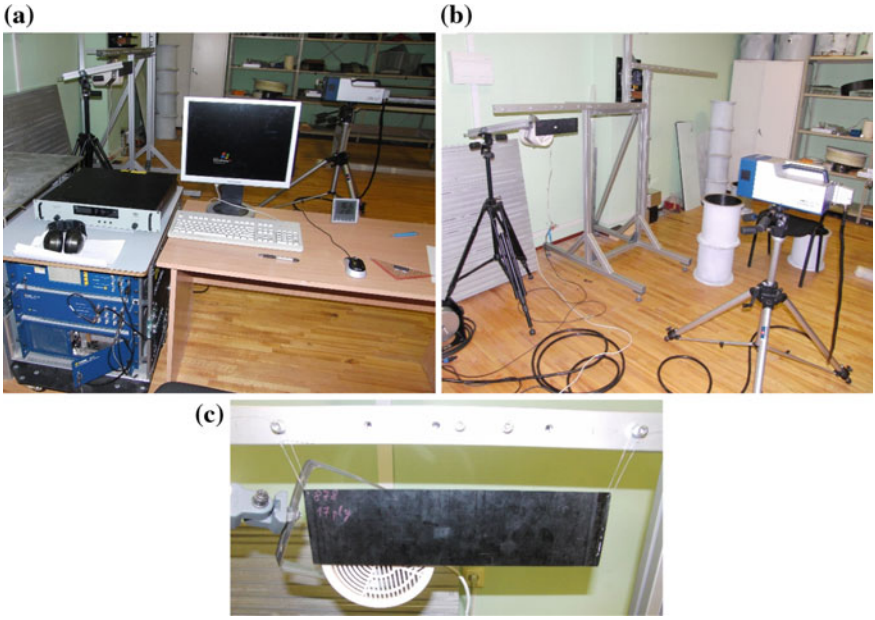

Fig. 1 Experimental set-up of vibration test: **a** overall view, **b** scanning head in the process of scanning the specimen, **c** close-up view of the plate specimen and loudspeaker

The dynamic testing of the plate involves measurement of its dynamic properties, namely, the resonance frequencies and corresponding deflection shapes. This procedure is carried out using a POLYTEC PSV-400-B non-contact scanning laser vibrometer. POLYTEC system consists of a PSV-I-400 LR optical scanning head equipped with a sensitive vibrometer sensor (OFV-505), OFV-5000 controller, PSV-E-400 junction box, a Bruel and Kjaer type 2732 amplifier, and a computer with a data acquisition board and PSV software (Fig. 1).

For the PSV acquisition system, it is required to define the location of outer edges of the specimen and then, a scanning grid, consisting of scanning points, uniformly distributed over the surface of specimen. Different geometries of scanning grid can be chosen along with a density of scanning points in either direction. Vibrations of a structure are measured in these points, in perpendicular direction to the surface of the structure. In this study, a rectangular grid has been chosen due to the rectangular shape of the specimen. The scanning grid of a composite plate consists of seven points on width and 21 points on length of the sample, yielding 147 scanning points in a whole.

Table 2 Specifications of dynamic testing

Signal	Periodic chirp with 9 V amplitude
Bandwidth	100 Hz–3.2 kHz
FFT lines	3101
Sample frequency	8.192 kHz
Resolution	1 Hz
Channel vibrometer voltage	10 V

The plate was suspended by thin threads, thus tested in the both edges free boundary conditions. A periodic chirp signal, generated by internal function generator, was passed to a loudspeaker to excite the plate. The scanning head measured a velocity of vibration in a scanning point and automatically moved the laser beam to a successive point of the scan grid. This measurement procedure involved validating the measurement with the signal-to-noise ratio. During the measurement, the photo-detector (highly sensitive digital decoder VD-07), measured the time-dependent vibration velocity. Then the measurements were performed; the time response of the plate, averaged 3 times at each point, was transformed to the frequency domain using Fast Fourier Transform yielding Frequency Response Function (FRF). The identification of resonance frequencies was conducted by using the peak picking method, studying FRF. The corresponding displacement deflection shapes were obtained by further post-processing of the data. Set-up parameters, used for the FRF measurements, are shown in Table 2.

At first, FRF was measured for a healthy plate that contained no damage. Two impacts of different severities and in different locations were carried out by using a low-velocity impact procedure. After each of impacts, FRF and deflection shapes were measured. The resonance frequencies and deflection shapes were not only used for comparison purposes, e.g., how damage affected the dynamic parameters of the structure, but deflection shapes also served as input data for our proposed damage localization algorithm.

3 Low-Velocity Impact Tests

Low-velocity impact tests were conducted using INSTRON Dynatup 9250 HV drop tower. Different impact energies were calculated by using the variation of impactor mass and drop height. The potential energy of the impactor at maximum height is transferred to a sample in the process of an impact. The impactor with hemispherical nose, a diameter of 20 cm and a mass of 2.25 kg was used in the test. In total, two impact tests with different energies were performed in order to assess the locations of damage with different severities.

The location of first impact with an energy of 5 J corresponds to orange circle in Fig. 2. After this impact, deflection shapes of the plate were measured. Then, the

Fig. 2 Photo of a composite plate with *orange* and *red rings* showing the location of 5 and 9 J impact damage, respectively (color figure online)

Table 3 Specifications of impact test

Impact no.	Impact energy (J)	Maximum load (kN)	Deflection at max load (mm)	Test height (m)	Impact velocity (m/s)
1	8.8383	5.6162	3.75	0.4532	2.8029
2	4.8986	3.7568	3.0091	0.2266	2.0867

second impact with an energy of 9 J was performed and its location is marked with a red circle in Fig. 2. After both impacts were made, the deflection shapes were measured one more time.

Details of impact testing set-up parameters are found in Table 3.

4 Damage Localization Methodology

In this chapter, location of damage in a CFRP plate is assessed by using two-dimensional CWT technique, which implies the use of so-called wavelets. Wavelets $\psi(t)$ are special functions with small oscillations, so that they have zero mean. Wavelets possess several distinctive properties, such as

- support width;
- may be orthogonal/biorthogonal;
- may be symmetric/asymmetric;
- the majority of wavelets are grouped in families, for example, Mexican Hat (mexh, esmexh, gabmexh), Derivative of Gaussian (dog, dog2, dog3), Morlet (morl, isomorl, esmorl, rmorl), etc.;
- may be isotropic or orthotropic in dependence on that how their properties depend on rotational angle in a plane.

Wavelet analysis is usually performed in time domain, meaning that they have a period and a frequency. This wavelet frequency is called central frequency of wavelet and it can be imagined as a frequency that wavelet would have if it has sinusoidal nature. Wavelet pseudo frequencies are obtained by dividing the central frequency with a scale factor s. The scale factor, also known as dilation parameter, is a real positive number, that depicts a compression $(0<s<1)$, when window function is very narrow, therefore it is appropriate for high-frequency components. On the other hand, a tension $(s>1)$ of wavelet function along abscissa axis gives rise to the very wide windows that are suitable for the low-frequency components of the signal [21, 22]. This concept is based on *Heisenberg uncertainty principle*, which states that it is not possible to obtain high resolution in frequency and time simultaneously [23]. WT can adopt a flexible time-frequency window, thus this method exceeds different Fourier transform sub-techniques [24]. Spatial wavelet analysis is performed, as the name implies, in spatial domain, simply replacing time with coordinate, giving rise to wavelet function $\psi(x,y)$ [25, 26].

In its nature, WT is a convolution of analyzed signal $f(x,y)$ with a wavelet function $\psi(x,y)$ [27] and measures actually a correlation between $f(x,y)$ and $\psi(x,y)$ [16]. For a given value of s, $\psi(x,y)$ translates along x and y axes and convolves with every segment of signal $f(x,y)$. Large magnitude transform coefficients indicate places with high degree of correlation and vice versa.

In the damage identification procedure, large Wavelet Transform coefficients appear as spikes in WT plots of y versus x. The coordinates that correspond to these spikes contain the location of damage because damage can be imagined as a discontinuity of a signal.

The 2D CWT for a two-dimensional signal is given by Alamdari et al. [28]

$$W_{s,a,b} = \frac{1}{\sqrt{s^2}} \iint f(x,y) \cdot \psi^* \left(\frac{x-a}{s}, \frac{y-b}{s} \right) \mathrm{d}x\mathrm{d}y = \iint f(x,y) \cdot \psi^*_{s,a,b}(x,y) \mathrm{d}x\mathrm{d}y, \tag{1}$$

where asterisk denotes complex conjugation and $\psi_{s,a,b}(x,y)$ is a set of wavelet family functions, derived from a mother wavelet function $\psi(x,y)$ by using translation (parameters a and b) and expansion (parameter s) of the $\psi(x,y)$.

Damage index for each of mode shapes is depicted as follows:

$$\mathrm{DI}^n_{i,j,s} = W^n_{i,j,s} = \iint_s w^n_{i,j} \cdot \psi^*_{s,a,b}(x,y) \mathrm{d}x\mathrm{d}y, \tag{2}$$

where S is the area of the plate, w^n is the transverse displacement of the structure, n is the mode number, i and j are the numbers of grid points in x and y directions, respectively. However, mode shapes, measured in experimental conditions, are always damaged by measurement noise, which may lead to false peaks in damage index profiles, thus misleading data interpretation. In order to overcome this problem, it is proposed to summarize the results for all modes. The summarized

damage index is then defined as the average summation of damage indices for all modes and normalized with respect to the largest value of each mode

$$\mathrm{DI}_{i,j,s} = \frac{1}{N}\sum_{n=1}^{N}\frac{DI_{i,j,s}^{n}}{\max\left(DI_{i,j,s}^{n}\right)}. \tag{3}$$

According to [12, 24], the damage indices, determined for each of elements, are then standardized as

$$\mathrm{SDI}_{i,j,s} = \frac{\mathrm{DI}_{i,j,s} - \mu_s}{\sigma_s}, \tag{4}$$

where μ_s and σ_s are scale-dependent mean value and standard deviation of damage indices in Eq. (3), respectively.

The detection of the most energetic features in the signal at different scale and space is of particular interest in damage identification. Such three-dimensional plots consisting of coefficients of CWT with respect to waveletscale and dimension of the structure are known as *wavelet scalograms* [21, 29]. More beneficial, however is a *normalized wavelet scalogram* (NWS), where WT coefficients are first normalized.

$$\mathrm{NSDI}_{i,j,s} = \frac{\mathrm{SDI}_{i,j,s}}{s^2} \tag{5}$$

$$\mathrm{NWS}_{i,j,s} = \mathrm{NSDI}_{i,j,s} * \mathrm{NSDI}_{i,j,s} = \left|\mathrm{NSDI}_{i,j,s}\right|^2 \tag{6}$$

Regions of maxima in NWS are called wavelet transform ridges, which in the case of spatial CWT correspond to a coordinate with the most energetic features of the signal. The ridges in NWS denote the location of damage for spatial CWT. In [30], it is stated that wavelet ridges might be used for monitoring of damage development in the structure.

Since there is no wavelet scalogram for a two-dimensional case, it is proposed in our damage identification methodology to compute a sum of NWS along x and y directions, giving rise to *summed normalized wavelet scalogram* θ that is only scale-dependent

$$\theta_s = \sum_{j}\sum_{i}\mathrm{NWS}_{i,j,s} \tag{7}$$

The next step is to calculate a percentage of energy that normalizes wavelet scalogram and contains at each scale with respect to summed normalized wavelet scalogram at each scale. It yields a new introduced variable, called *fractional normalized wavelet scalogram* $\mathsf{C}_{i,j,s}$ as follows

$$\mathbb{C}_{i,j,s} = 100\% * \frac{\mathrm{NWS}_{i,j,s}}{\mu(\theta_s)} = 100\% * \frac{\mathrm{NWS}_{i,j,s}}{\mu\left(\sum_j \sum_i \mathrm{NWS}_{i,j,s}\right)}, \tag{8}$$

where $\mu(\theta_s)$ denotes the mean value of θ.

The next step of calculations involves the computation of a damage index that is obtained by taking into account a variance of fractional normalized wavelet scalogram with respect to scale parameter, thus eliminating the scale variable from the damage localization procedure

$$\Gamma_{i,j} = \sigma^2\left(\mathbb{C}_{i,js}\right) = \sigma^2\left(100\% * \frac{\mathrm{NWS}_{i,j,s}}{\mu\left(\sum_j \sum_i \mathrm{NWS}_{i,j,s}\right)}\right) \tag{9}$$

The variable $\Gamma_{i,j}$ depends only on coordinates of the plate.

It is unknown a priori, which wavelet functions will be used better in different cases, therefore, it is proposed to define the localization of damage on pairs of highly correlated wavelets. This procedure is organized as follows:

- We calculate $\Gamma_{i,j}$ for all of the wavelet functions and analyze a *cross-correlation* of these values between all wavelets.
- Wavelet pairs with high correlation coefficient are extracted from the list of all wavelets. For all of these pairs, the average value of $\Gamma_{i,j}$ is calculated from individual $\Gamma_{i,j}$ of each wavelet in pair. For example, for the first and second highly correlated wavelet pairs, the average value of $\Gamma_{i,j}$ is computed as follows

$$\Gamma^1_{i,j} = 0.5 \cdot \left(\Gamma^{1,1}_{i,j} + \Gamma^{1,2}_{i,j}\right), \Gamma^2_{i,j} = 0.5 \cdot \left(\Gamma^{2,1}_{i,j} + \Gamma^{2,2}_{i,j}\right) \tag{10}$$

- If k is number of highly correlated wavelet pairs, then the *average correlated variance of normalized wavelet scalogram* (ACVNWS) is computed as

$$\overline{\Gamma_{l,j}} = \frac{1}{k}\sum_k \Gamma^k_{i,j} \tag{11}$$

- By considering the problem of damage localization, it is proposed to extract the values of $\overline{\Gamma_{i,j}}$ by applying an *universal wavelet threshold*

$$T = \sigma\sqrt{2\ln(N)}, \tag{12}$$

where N in our case is the total number of data points and σ is the standard deviation of $\overline{\Gamma_{i,j}}$ distribution over plate. Originally, this threshold was adapted in image noise reduction routine by using wavelets [31–33].

- In the following calculations, the values of $\overline{\Gamma_{i,j}}$ that do not pass the threshold value of T, are assigned a value of zero, otherwise these values are assigned a value of 1, forming a distribution of *thresholded average correlated variance of normalized wavelet scalogram* (TACVNWS):

$$\begin{aligned} \text{if}\left(\overline{\Gamma_{i,j}} \ll T\right) &\rightarrow T\overline{\Gamma_{i,j}} = 1 \\ \text{else} &\rightarrow T\overline{\Gamma_{i,j}} = 0 \end{aligned} \tag{13}$$

5 Results and Discussion

The frequency response functions (FRFs) for damage cases of 5 J impact and additional 9 J impact, measured in a vibration test are shown in Fig. 3. For a reference, FRF of a healthy plate is also plotted.

Deflection shapes are extracted from FRFs and their amplitude is normalized to unity. In a whole, 12 deflection shapes are extracted from a healthy plate in the case with impact of 5 J and 16 shapes—in the case of combined 5 and 9 J impact damage. However, only the corresponding shapes are used in further calculations. The pairs of corresponding deflection shapes of the both damage cases are determined by using a correlation coefficient. A value close to 1 or −1 indicates a correlation between these shapes. As a result, nine pairs of corresponding deflection shapes are identified and three of these pairs are shown in Fig. 4.

Resonance frequencies, corresponding to identified pairs of deflection shapes are depicted in Table 4. As expected, the presence of damage lowers the values of resonance frequencies and this effect is more pronounced at higher resonances.

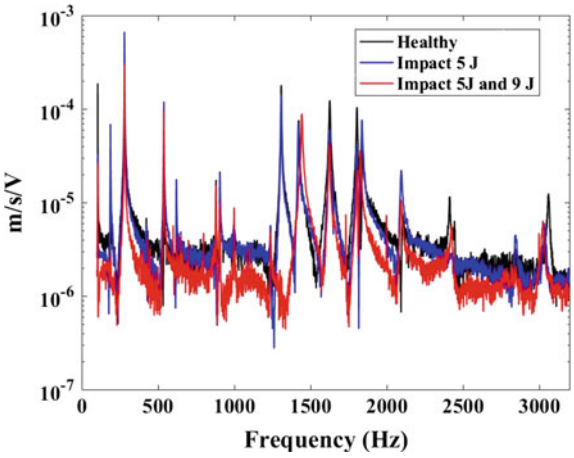

Fig. 3 Frequency response functions for two damage cases

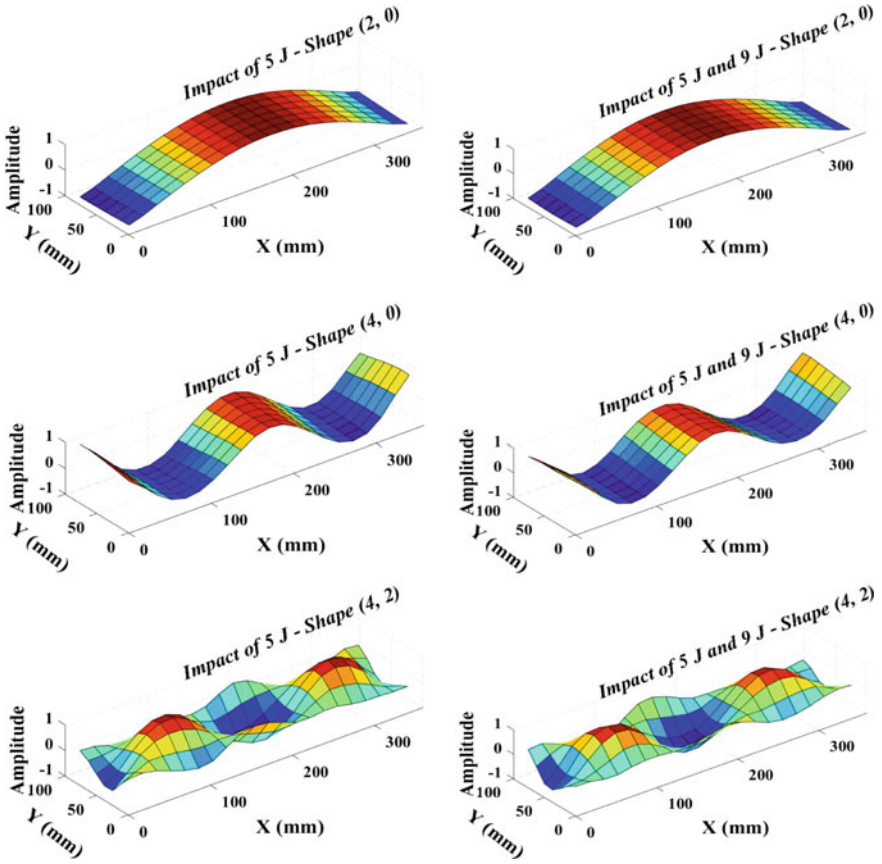

Fig. 4 Deflection shapes measured in dynamic tests for a composite plate containing 5 J and 5 J + 9 J impact damage

Table 4 Resonance frequencies of composite plate

Shape	Healthy	Impact 5 J	Impact 5 J + 9 J	Correlation coefficient
(2, 0)	105	105	105	0.994641
(1, 1)	188	188	189	0.987661
(3, 0)	280	280	280	0.979836
(4, 0)	539	539	539	0.962761
(3, 1)	622	621	620	−0.92806
(4, 1)	906	906	880	−0.80034
(2, 2)	1627	1626	1624	0.95612
(4, 2)	2101	2096	2094	0.84852
(9, 0)	3062	3036	3027	−0.88688

Also, the correlation coefficient is given and negative values with a magnitude close to 1 depict a phase shift of corresponding shapes in the moment of extraction.

The cross-correlation results of $\Gamma_{i,j}$ values between all 16 wavelets are shown in Fig. 5. The dark regions in cross-correlation maps represents low or no correlation, while white regions represent high correlation as indicated by the colorbar.

The selection of wavelet pairs then used in $\overline{\Gamma_{i,j}}$ calculation is based on a threshold of correlation results. Basically, wavelet pairs, which performance exceeds a correlation threshold of 0.895 are selected for further analysis. The pairs exceeding this threshold are assigned by value of 1, otherwise 0, forming a matrix of zeros and ones, named *correlated average variance of normalized wavelet scalogram pairs* $C\overline{\Gamma_{i,j}}$

$$\begin{aligned} \text{if}\left(\rho_{xy}\overline{(\Gamma_{i,j})} \ll 0.895\right) \rightarrow C\overline{\Gamma_{i,j}} = 0 \\ \text{else} \rightarrow C\overline{\Gamma_{i,j}} = 1, \end{aligned} \tag{14}$$

where $\rho_{x,y}$ is a correlation coefficient between pairs of $\overline{\Gamma_{i,j}}$ values for wavelets.

Each wavelet function with a short-hand name from MATLAB R2016B is assigned a number from 1 to 16, as shown in Table 5. The results of cross-correlation between wavelets in Table 5 are shown in Tables 6 and 7. These $C\overline{\Gamma_{i,j}}$ matrices are built for both cases of damage (5 and 9 J). It is worth noting that

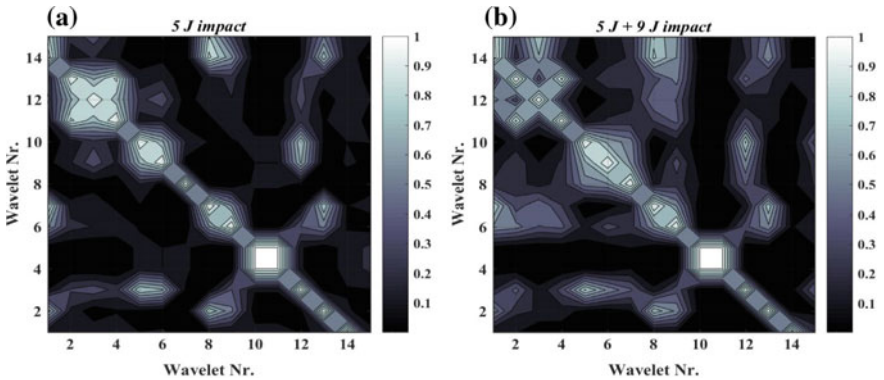

Fig. 5 Correlation maps of variances of SDI between all wavelets: **a** impact of 5 J, **b** impacts of 5 J + 10 J

Table 5 Numerical notation of wavelet functions used in algorithm

1	2	3	4	5	6	7	8
pethat	isomorl	rmorl	esmorl	morl	dog	Dog2	isodog
9	10	11	12	13	14	15	16
fan	wheel	gaus3	gaus2	mexh	esmexh	gabmexh	sinc

Table 6 $C\overline{\Gamma_{ij}}$ matrix for the case of 5 J impact

0	0	0	0	0	0	0	0	0	0	0	0	0	0	0
1	0	0	0	0	0	0	1	0	0	0	0	0	0	0
0	1	0	1	0	0	0	0	0	0	0	0	0	0	0
0	0	1	0	0	0	0	0	0	0	0	0	0	0	0
0	1	0	1	0	0	0	0	0	0	0	0	0	0	0
0	0	0	0	1	0	0	0	0	0	0	0	0	0	0
0	0	0	0	0	1	0	0	0	0	0	0	0	0	0
0	0	0	0	0	0	1	0	0	0	0	0	0	0	0
1	0	0	0	0	0	0	1	0	0	0	0	0	0	0
0	0	0	0	0	0	0	0	1	0	0	0	0	0	0
0	0	0	0	0	0	0	0	0	1	1	0	0	0	0
0	0	0	0	0	0	0	0	0	1	1	0	0	0	0
0	0	0	0	0	0	0	0	0	0	0	1	0	0	0
1	0	0	0	0	0	0	1	0	0	0	0	1	0	0
0	0	0	0	0	0	0	0	0	0	0	0	0	1	0

Table 7 $C\overline{\Gamma_{ij}}$ matrix for the case of 5 J + 9 J impact

1	0	0	0	0	0	0	0	0	0	0	0	0	0	0
1	0	0	0	0	0	0	0	0	0	0	0	0	0	0
0	1	0	1	0	0	0	0	0	0	0	0	0	0	0
0	0	1	0	0	0	0	0	0	0	0	0	0	0	0
0	1	0	1	0	0	0	0	0	0	0	0	0	0	0
0	0	0	0	1	0	0	0	0	0	0	0	0	0	0
0	0	0	0	0	1	0	0	0	0	0	0	0	0	0
0	0	0	0	0	0	1	0	0	0	0	0	0	0	0
1	0	0	0	0	0	0	1	0	0	0	0	0	0	0
0	0	0	0	0	0	0	0	1	0	0	0	0	0	0
0	0	0	0	0	0	0	0	0	1	1	0	0	0	0
0	0	0	0	0	0	0	0	0	1	1	0	0	0	0
0	0	0	0	0	0	0	0	0	0	0	1	0	0	0
1	0	0	0	0	0	0	1	0	0	0	0	1	0	0
0	0	0	0	0	0	0	0	0	0	0	0	0	1	0

these matrices are symmetric, thus botton part of the matrices is shaded gray. The main diagonal is shaded red because the cross-correlation is performed between a particular wavelet and itself, so those values of one do not contribute to the selection of wavelet pairs. The cases, where the cross-correlation has passed the threshold, are shaded green.

As one can see, a total of three pairs of wavelets have passed the cross-correlation threshold for each of two damage cases. These wavelet pairs are given in Table 8.

Table 8 Wavelet pairs used in the calculation of $\overline{\Gamma_{i,j}}$ for both cases of damage

isomorl-fan	5 J impact	pethat-isomorl	5 J + 9 J impact
rmorl-morl		rmorl-morl	
gaus2-gaus3		gaus2-gaus3	

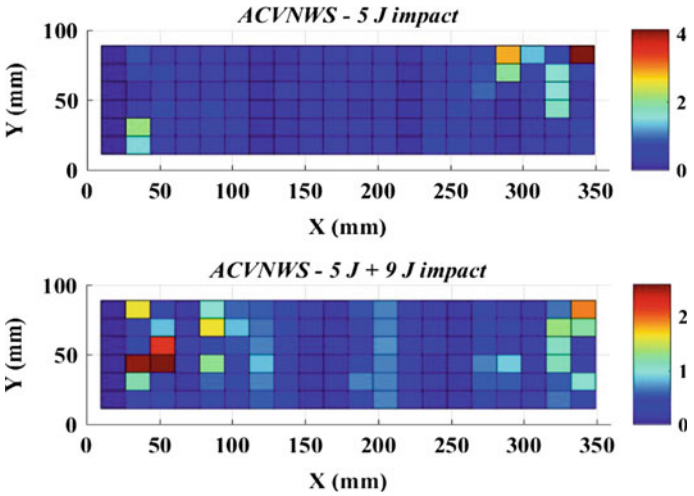

Fig. 6 Average correlated variance of normalized wavelet scalogram distributions for both damage cases

The $\overline{\Gamma_{i,j}}$ distributions over the surface of a composite plate by using the selected wavelet pairs are computed with help of Eq. (11) and shown in Fig. 6.

For the case of 5 J impact, elevated values are located at the upper right corner of the plate and at the left, where the actual impact was made. However, moderate values are also found in the bottom left region no contributing to damage. In the 5 J + 9 J impact case, the highest values are found on the far left side of the plate in the vicinity of damage.

Universal threshold, according to Eq. (12) is applied to the distributions in Fig. 7. The calculated values for the universal threshold are shown in Table 9.

The values of T in Table 8 mean that if the values from Fig. 6 are larger than calculated values of T, they are assigned by value of 1. If values from Fig. 6 are smaller that T, they are set to zero. These distributions of threshold values of $\overline{\Gamma_{i,j}}(T\,\overline{\Gamma_{i,j}})$ are shown in Fig. 7.

Although smaller values of $\overline{\Gamma_{i,j}}$ distributions are extracted, there are still some higher values in the profile that no contribute to the damage. In the case of 5 J impact, such values locate in the left part and at the top right corner of the plate, while in the case of 5 J + 9 J impact, these values at the top right and left corners of the plate.

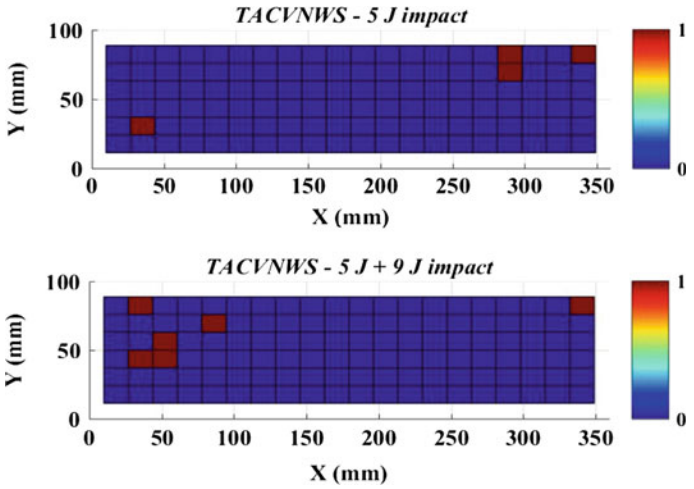

Fig. 7 Threshold average correlated variance of normalized wavelet scalogram distributions for both damage cases

Table 9 Values of universal threshold for both damage cases

T	5 J impact	5 J + 9 J impact
	1.7398	1.4749

Two values for the case of 5 J impact locate close one to other in the location of impact damage in the top right part of the plate and three neighboring values locate in the left part of the plate for 5 J + 9 J impact case in the approximate location of damage, suggesting that, in general, the proposed methodology is capable to localize impact damage even at small severity (5 J). However, in the case of 5 J + 9 J impact, only largest severity damage (9 J) is localized properly.

6 Conclusions

This study is devoted to localization of impact damage in thin ($\sim$2 mm) composite plate. Two successive impacts with severities of 5 and 9 J are applied by using low-velocity impactor and resonance frequencies along with corresponding deflection shapes of the plate are measured in a dynamic vibration test. These shapes are used as input data in a damage localization algorithm by using 2-D Continuous Wavelet Transform. Variance of normalized wavelet scalogram is calculated over the scale parameters for each of 16 wavelets considered in the study, thus excluding the scale out of the variables in damage localization problem. The problem of selection of the most appropriate wavelet function is solved by the

cross-correlation between performances of all wavelets, and the most highly correlated wavelet pairs are selected. These pairs are used in the calculation of damage index distributions over the plate. Universal threshold is applied in order to extract the lowest magnitude values that no contribute to damage.

According to final damage localization results, the proposed methodology is successful, although some discrepancy is present, especially in the case with damage of both severities because in this case the algorithm detects only the highest severity damage.

Acknowledgements This research has been performed under the funding from the Latvia State Research Programme, the grant agreement "Innovative Materials and Smart Technologies for Environmental Safety, IMATEH".

References

1. D. Ginzburg, F. Pinto, O. Iervolino, M. Meo, Compos. Struct. **161**, 187 (2017)
2. E. Stelldinger, A. Kühhorn, M. Kober, Compos. Struct. **139**, 30 (2016)
3. T.O. Topac, B. Gozluklu, E. Gurses, D. Coker, Compos. A **92**, 167 (2017)
4. R. Toivola, P.-N. Lai, J. Yang, S.-H. Jang, A.K.-Y. Jen, B.D. Flinn, Compos. Sci. Technol. **139**, 74 (2017)
5. Y. Li, W. Zhang, Z.-W. Yang, J.-J. Zhang, S.-J. Tao, Infrared Phys. Technol. **76**, 91 (2016)
6. V.B. Dawari, G.R. Vesmawala, Proc. Eng. **51**, 119 (2013)
7. P. Qiao, K. Lu, W. Lestari, Wang. J Compos. Struct. **80**, 409 (2007)
8. P. Qiao, W. Lestari, Compos. Struct. **67**, 365 (2005)
9. M. Dilena, A. Morassi, Mech. Syst. Signal Process. **25**, 1485 (2011)
10. M. Cao, L. Ye, L. Zhou, Z. Su, R. Bai, Mech. Syst. Signal Process. **25**, 630 (2011)
11. J.-M. Ndambi, J. Vantomme, K. Harri, Eng. Struct. **24**, 501 (2002)
12. J.-T. Kim, Y.-S. Ryu, H.-M. Cho, N. Stubbs, Eng. Struct. **25**, 57 (2003)
13. A. Katunin, F. Holewik, Arch. Civil Mech. Eng. **13**, 287 (2013)
14. A. Katunin, P. Przystałka, Eng. Appl. Artif. Intell. **30**, 73 (2014)
15. A. Katunin, Mech. Syst. Signal Process. **25**, 3153 (2011)
16. A. Katunin, Arch. Civil Mech. Eng. **15**, 251 (2015)
17. A. Katunin, Compos. Struct. **118**, 385 (2014)
18. P. Qiao, W. Fan, Int. J. Solids Struct. **46**, 4379 (2009)
19. Y. Huang, D. Meyer, S. Nemat-Nasser, Mech. Mater. **41**, 1096 (2009)
20. Y.J. Yan, L.H. Yam, Compos. Struct. **58**, 29 (2002)
21. P.S. Addison, *The Illustrated Wavelet Transform Handbook, Introductory Theory and Applications in Science, Engineering, Medicine and Finance* (Taylor & Francis, New York-London, 2002)
22. H. Adeli, H. Kim, *Wavelet-Based Vibration Control of Smart Buildings and Bridges* (CRC Press, Taylor and Francis Group, Boca Raton, London, New York, 2009)
23. H. Kim, H. Melhem, Eng. Struct. **26**, 347 (2004)
24. W.L. Bayissa, N. Haritos, S. Thelandersson, Mech. Syst. Signal Process. **22**, 1194 (2008)
25. C.-C. Chang, L.-W. Chen, Mech. Syst. Signal Process. **19**, 139 (2005)
26. N. Wu, Q. Wang, Int. J. Eng. Sci. **49**, 253 (2011)
27. Y.F. Xu, W.D. Zhu, J. Liu, Y.M. Shao, J. Sound Vib. **333**, 6273 (2014)

28. M.M. Alamdari, J. Li, B. Samali, Arch. Civil Mech. Eng. **15**, 698 (2015)
29. S. Goswami, P. Bhattacharya, Int. Res. J. Eng. Technol. **2**(3), 2060 (2015)
30. M.M.R. Taha, A. Noureldin, J.L. Lucero, T.J. Baca, Struct. Health Monit. **5**(3), 267 (2006)
31. V. Sowjanya, G. SasibhushanaRao, A. Sarvani, Proc. Comput. Sci. **85**, 669 (2016)
32. A. Azzalini, M. Farge, K. Schenider, Appl. Comput. Harmon Anal **18**, 177 (2005)
33. X. Zhang, N. Feng, Y. Wang, Y. Shen, J. Sound Vib. **339**, 419 (2015)